ACS OMEGA

http://pubs.acs.org/journal/acsodf

Article

Study on PQ/PMMA Photopolymer Films Fabricated by Solvent Casting

Yu-Hsiang Hsieh, Yung-Cheng Cheng, and Te-yuan Chung*

Cite This: *ACS Omega* 2022, 7, 11770−11776

Read Online

ACCESS | Metrics & More | Article Recommendations

ABSTRACT: PQ/PMMA photopolymer films fabricated by solvent casting are realized using tetrahydrofuran (THF) as the solvent. The corresponding photochemical reaction model is established with material parameters numerically studied based on 57 samples recorded with a 532 nm laser. The fabrication and the recording time are noticeably reduced. A 2-fold increase in the average refractive index variation is achieved compared with the two-step thermal polymerization method with the same PQ initial concentration.

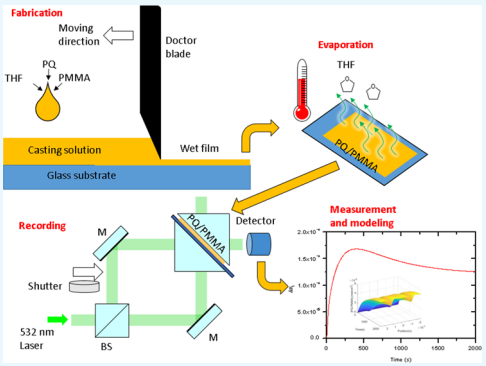

1. INTRODUCTION

PQ (9,10-phenanthrenequinone)-doped PMMA (polymethyl methacrylate), PQ/PMMA, was first reported by Steckman et al. in 1998[1] as the easy-to-make holographic recording material with low shrinkage and low cost.[1−7] In 2000, Lin et al. developed the method of two-step thermal polymerization and fabricated the bulk material of PQ/PMMA with large dimensions.[2] In 2008, Luo et. al exposed PQ/PMMA to a periodic light field to make a transmission volume Bragg grating (VBG) of 90% diffraction efficiency for a spectral-spatial imaging filter.[8] In 2014, a reflective PQ/PMMA VBG serving as the laser mirror of a 976 nm tapered amplifier successfully achieved a high-power single-mode laser.[9] In 2011, Liu et al. proposed the photochemical reaction mechanisms and model of the recording process of PQ/PMMA. The corresponding rate equations were established.[10] In 2016, Shih et al. simplified the model by assuming that MMA monomers are abundant and the change of MMA concentration can be neglected during the recording process.[11]

However, the previous models for the two-step thermal polymerization method requiring the assumption of a constant concentration of residual MMA monomers throughout the recording process might be inadequate to estimate the actual amount of the photoproduct. Also, the time-consuming fabrication process of the two-step thermal polymerization method usually takes up to 36 h before the sample can be recorded.

This work utilizes the solvent casting method frequently adopted in fabricating organic semiconductor thin films[12] for PQ/PMMA fabrication. Dissolving ready-made PMMA and PQ with tetrahydrofuran (THF), practically no MMA monomers are left in the sample. The corresponding photochemical reaction model and the reaction rate and diffusion equations are proposed. A series of simulations and experiments were performed to evaluate the unknown material parameters of different fabrication and recording conditions.

2. MODELING

The photochemical reaction model utilizing differential equations to evaluate molecular concentrations as a function of space and time describes the dynamic behavior of PQ molecules excited by photons, the diffusion through the PMMA matrix, and the reactions with PMMA molecules. By applying the Lorentz−Lorenz formulation, the refractive index distribution can be evaluated with the knowledge of molecular concentrations. With a periodic recording pattern, the diffraction efficiency can then be obtained by the coupled-wave theory.

2.1. Reaction Rate and Diffusion Equations. PQ molecules can be excited by blue-green photons, and the corresponding reaction[10] can be written as

Received: December 6, 2021
Accepted: March 4, 2022
Published: March 28, 2022

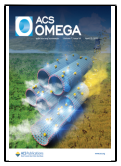

$$PQ + h\nu \xrightarrow{k^{PQ}} {}^1PQ^* \xrightarrow{k_{^1PQ^*}} {}^3PQ^* \quad (1)$$

where $h\nu$ represents the absorbed photon, k_{PQ} indicates the excitation rate of PQ to ^{1}PQ*, and $k_{^1PQ^*}$ is the transfer rate of ^{1}PQ* to ^{3}PQ*. k_{PQ} can be expressed as

$$k_{PQ} = \sigma_{PQ}\frac{I}{h\nu} \quad (2)$$

where σ_{PQ} is the effective absorption cross section of PQ in the PMMA matrix. I and ν are the intensity and frequency of the recording light, respectively. The singlet state ^{1}PQ* promptly turns into the triplet state ^{3}PQ* that has an extremely long lifetime; therefore, ^{1}PQ* can be neglected in the reaction rate and diffusion equations. ^{3}PQ* can react with a hydrogen atom on a PMMA chain and attaches to the chain at the same site.[10] The reactions are described by

$${}^3PQ^* + RH \xrightarrow{k_i} HPQ^\bullet + R^\bullet \quad (3)$$

$$HPQ^\bullet + R^\bullet \xrightarrow{k_t} HPQR \quad (4)$$

where k_i and k_t are the corresponding reaction rates, R represents the rest of the PMMA chain, and HPQR is known as the PQ/PMMA molecule. The second reaction happens much faster than the first one;[10] therefore, eqs 3 and 4 can be reduced to

$${}^3PQ^* + PMMA \xrightarrow{k_i} PQ/PMMA \quad (5)$$

Note that ^{3}PQ* molecules travel freely through the openings inside the PMMA matrix; therefore, only the hydrogen atoms exposed to the void of the PMMA matrix that can make contact with ^{3}PQ* are able to participate in the reactions. As a result, PMMA in eq 5 will be referred to as react-able hydrogen, H_{react}, in the following paragraphs. Also, the large molecular weights of PMMA and PQ/PMMA, which are more than a million, along with the tangled PMMA chains make the diffusion of PMMA and PQ/PMMA negligible. Therefore, the reaction rate and diffusion equations can be written by simplifying the model in ref 10 as

$$\frac{\partial[PQ(x,t)]}{\partial t} = \frac{\partial}{\partial x}D_{PQ}\frac{\partial[PQ(x,t)]}{\partial x} - k_{PQ}[PQ(x,t)] \quad (6)$$

$$\frac{\partial[{}^3PQ^*(x,t)]}{\partial t} = \frac{\partial}{\partial x}D_{^3PQ^*}\frac{\partial[{}^3PQ^*(x,t)]}{\partial x} + k_{PQ}[PQ(x,t)] - k_i[{}^3PQ^*(x,t)][H^{react}(x,t)] \quad (7)$$

$$\frac{\partial[H^{react}(x,t)]}{\partial t} = -k_i[{}^3PQ^*(x,t)][H^{react}(x,t)] \quad (8)$$

$$\frac{\partial[PQ/PMMA(x,t)]}{\partial t} = k_i[{}^3PQ^*(x,t)][H^{react}(x,t)] \quad (9)$$

where t is the time, x stands for the x-coordinate of the space, square parentheses represent the molarity of each kind of molecule enclosed, and D is the diffusion coefficient. With the above equations, the numerical method can be applied to model the dynamic spatial behaviors of the chemical reactions.

2.2. Refractive Index Variation and Diffraction Efficiency. The refractive indices of PQ, PMMA, and PQ/PMMA are 1.701, 1.493, and 1.497, respectively. With the above photochemical reactions, the exposed part of PQ/PMMA can lead to localized refractive index reduction.[2,10,11,13,14] Therefore, the periodic refractive index variation within PQ/PMMA can be achieved by the two-beam interference recording scheme.

PQ, ^{3}PQ*, and PQ/PMMA are the chemical compounds responsible for the refractive index distribution in this system. With the initial chemical concentrations and the recording intensity distribution, the reaction rate and diffusion equations give the spatial distributions of the chemical compounds at any given time. Similar to ref 11, the first-order Fourier coefficients of the chemical compound concentrations and Lorentz–Lorenz formulation[15] are applied. The overall refractive index variation of the first Fourier order can be written as

$$\Delta n_1(t) = \gamma_{PQ}A_{PQ}(t) + \gamma_{^3PQ^*}A_{^3PQ^*}(t) + \gamma_{PQ/PMMA}A_{PQ/PMMA}(t) \quad (10)$$

where γ is the proportionality constant of each chemical compound concentration and the corresponding contribution to the local refractive index of PQ/PMMA. A represents the first-order Fourier coefficients of each chemical compound concentration. With $\Delta n_1(t)$, the diffraction efficiency, $\eta(t)$, can be obtained by the coupled-wave theory.[16]

3. SIMULATIONS

3.1. Material and Recording Parameters. The simulation parameters fall into two categories, the material parameters and the recording parameters. Table 1 lists the material parameters. The lower case $_i$ after the square parentheses indicates the initial concentration of the corresponding molecules; n is the average refractive index of PQ/PMMA; $[PQ]_i$ and the grating thickness d are set to match the experimental conditions that will be discussed later; σ_{PQ} and D_{PQ} are set to the values in accordance with refs 11, 14, 17; and $D_{^3PQ^*}$, $[H_{react}]_i$, k_i, and γ cannot be obtained directly and will be determined by experimental results.

Table 1. Material Parameters

parameter	value (unit)	parameter	value (unit)
$[PQ]_i$	5.61×10^{-5} mol/cm^3	$[H_{react}]_i$	1×10^{-4} mol/cm^3
d	120 μm	k_i	20 cm^3/(mol·s)
σ_{PQ}	7.5×10^{-21} cm^2	γ_{PQ}	14 cm^3/mol
D_{PQ}	1.24×10^{-18} m^2/s	$\gamma_{^3PQ^*}$	16 cm^3/mol
$D_{^3PQ^*}$	1.24×10^{-18} m^2/s	$\gamma_{PQ/PMMA}$	37 cm^3/mol
n	1.493		

The recording parameters include the wavelength λ_0, the average intensity I_0 of the light source, the angle between the two recording beams θ_r, and the exposure time t_{ex}. Note that diffusion is a slow process; therefore, the simulation time is much longer than t_{ex} to reach equilibrium. The values listed in Table 2 are based on the experimental configurations. The recorded grating period in the sample is then determined to be 251.96 nm.

3.2. Dynamic Behaviors of Molecular Concentrations and Refractive Index Variations. Using the RK4 (Runge–Kutta) method, the time development of the reaction and diffusion equations can be evaluated. The temporal and spatial distributions of [PQ], [^{3}PQ*], and [PQ/PMMA] with t_{ex} = 50 s are shown in Figure 1. The corresponding first-order Fourier coefficients of these molecular concentrations as a function of t

https://doi.org/10.1021/acsomega.1c06887
ACS Omega 2022, 7, 11770−11776

Table 2. Recording Parameters

parameter	value (unit)
I_0	1.6 W/cm^2
λ_0	532 nm
θ_r	90°
t_{ex}	~50 s

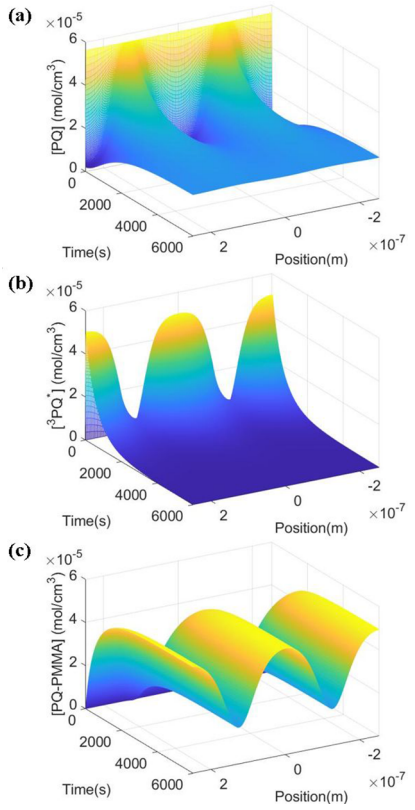

Figure 1. Simulation of the time-varying (a) [PQ], (b) [^{3}PQ*], and (c) [PQ/PMMA] concentration distributions of t_{ex} = 50 s recording.

can be calculated, as shown in Figure 2a. $\Delta n_1(t)$, shown in Figure 2b, and $\eta(t)$ can then be obtained by means of the Lorentz−Lorenz formulation and the coupled-wave theory.

The diffusion of PQ and ^{3}PQ* and the reaction of ^{3}PQ* and H_{react} are responsible for the development of Δn_1 after the exposure stops. Δn_f is defined as the final value of Δn_1 when diffusion and all reactions cease. By varying t_{ex}, Δn_f can be obtained, as shown in Figure 3. The peak of Δn_f located at about t_{ex} = 40 s is marked by the dashed line in the inset of Figure 3. When t_{ex} is less than 40 s, there are not enough PQ molecules that can be excited to form ^{3}PQ*, which leads to a smaller number of PQ/PMMA as well as a lower Δn_f. On the other hand, when t_{ex} is over 40 s, the first-order Fourier coefficient of [PQ/PMMA] gradually becomes smaller as discussed in ref 12 and results in a lower Δn_f. To ensure that the sample reaches the maximum diffraction efficiency, t_{ex} is chosen to be 60 s in the following simulations as well as the experiments. With the given laser intensity of 1.6 W/cm^2, the exposure fluence is 96 J/cm^2.

3.3. Analysis of the Material Parameters, k_i and $[H_{react}]_i$. In practice, higher Δn_1 and Δn_f are preferred. The influences of k_i and $[H_{react}]_i$ to Δn_1 can be simulated, as shown in Figure 4. Since $[^3PQ^*]_i$ distribution matches the recording light pattern and higher k_i allows ^{3}PQ* to react locally, [PQ/PMMA] matches better with the recording light pattern with higher k_i, which gives higher Δn_f, as shown in Figure 4a. On the other hand, higher $[H_{react}]_i$ increases the opportunity of ^{3}PQ* being intercepted by H_{react} during diffusion. Consequently, [PQ/PMMA] distribution also matches better with the recording light pattern. Higher Δn_f is thus achievable, as indicated in Figure 4b.

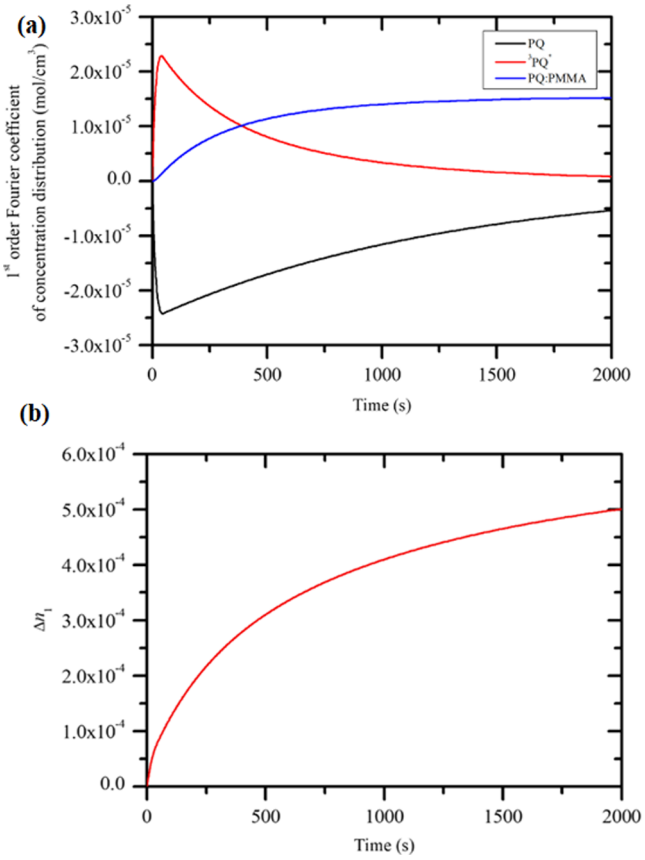

Figure 2. (a) First-order Fourier coefficient of each chemical compound concentration distribution and (b) $\Delta n_1(t)$ with t_{ex} = 50 s recording.

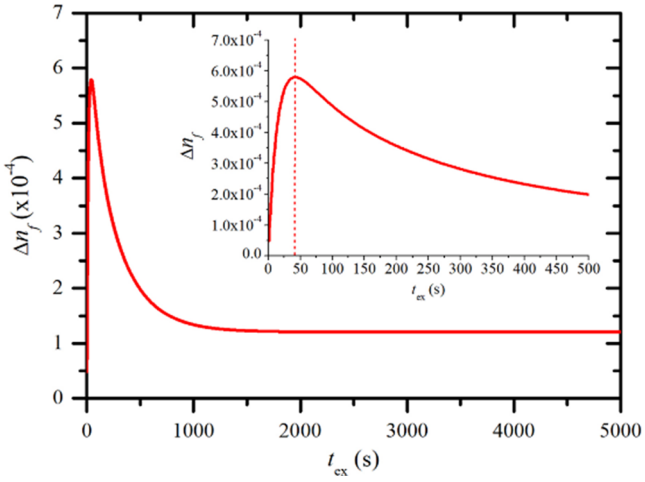

Figure 3. Δn_f as a function of t_{ex}.

https://doi.org/10.1021/acsomega.1c06887
ACS Omega 2022, 7, 11770−11776

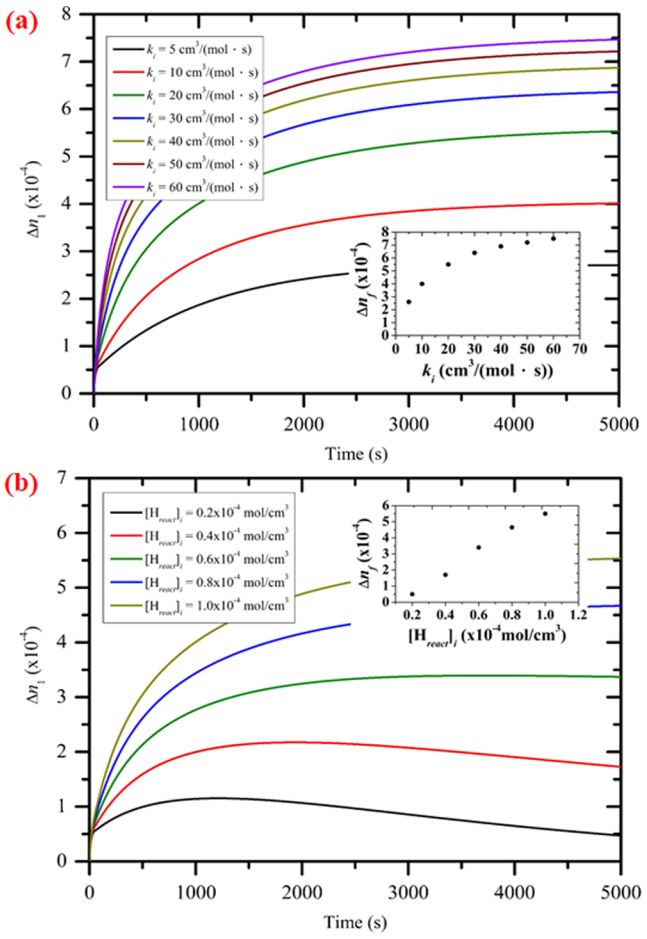

Figure 4. Δn_1 of 60 s recording: (a) k_i varies from 5 to 60 cm^3/(mol·s) and $[H_{react}]_i$ is set to 1×10^{-4} mol/cm^3. (b) $[H_{react}]_i$ varies from 0.2 $\times 10^{-4}$ to 1×10^{-4} mol/cm^3 and k_i is set to 60 cm^3/(mol·s). The insets are the final Δn_1 versus k_i and $[H_{react}]_I$, respectively.

4. FABRICATION AND RECORDING CONFIGURATIONS

4.1. Fabrication of a PQ/PMMA Film by Solvent Casting. The method of solvent casting involves three major procedures that include preparation of the casting solution, coating process, and evaporation. The casting solution consisted of 23.02 wt% PMMA powder (Merck & Co., average molecular weight of 120,000) as the host material and 0.23 wt% PQ (Tokyo Chemical Industry) as the additive that were dissolved by 76.75 wt% tetrahydrofuran (THF, Chung Yuan Chemicals). The mixture was stirred at a rate of 180 rpm at 45 °C for 120 min using a heating magnetic stirrer (Thermo Fisher Scientific, SP131325Q). The doctor blade coating method[12] was utilized to fabricate the film. About 2.5 mL of casting solution was spread by a doctor blade coater (KTQ-II) to form a 400 μm wet film on a BK7 substrate. The wet film was then placed inside a temperature-controlled environment for a 90 min evaporation process. The evaporation temperatures, T_{evap}, were chosen to be 60, 40, 25, or 5 °C, which may affect the morphology and characteristics of the film.[18−21] As shown in Figure 5, a solid film formed after THF evaporated, and the thickness of the film was measured to be 120 ± 10 μm. The absorption at the recording wavelength is about 4%. Regardless of the T_{evap}, the films showed excellent transparency with no noticeable scattering or surface roughness. The PQ/PMMA solid film and the BK7 substrate will be referred to as the sample in the following paragraphs.

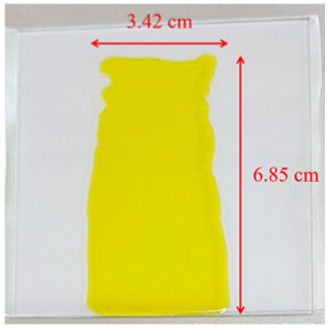

Figure 5. PQ/PMMA solid film after the evaporation process.

The entire fabrication process can be completed within 4 h, which is greatly reduced compared to the method of two-step thermal polymerization.[2] Furthermore, ready-made PMMA powder is used instead, and the difficulty of estimating the residual MMA monomer concentration is thus avoided.

4.2. Two-Beam Interference Recording Configuration. The recording configuration is shown in Figure 6. A single longitudinal mode 532 nm laser (Coherent, Verdi) was chosen to be the recording light source. A Faraday isolator (Optics for Research, IO-5-532-LP) was used to prevent optical feedback. The polarization was then adjusted by a half-wave plate to TE polarization with respect to the surface of the sample. To increase the spatial coherence, a spatial filter composed of a 20 × objective (Thorlabs, RMS20X) and a 10 μm pinhole (Thorlabs, P10H) was mounted before a collimation lens (Thorlabs, C330TME). The laser beam was split with a 50:50 beamsplitter (Thorlabs, BS013). M5 and M6 redirect the two recording beams to the sample. The angle between the two recording beams was set to be 90°. The sample was clamped by two BK7 right-angle prisms (Thorlabs, PS912) whose refractive indices are 1.52. Silicone oil (Kuen Min Tech) of refractive index 1.52 was applied to both surfaces of the sample for refractive index matching.

The diffraction efficiency of the sample during the recording process was monitored and measured by blocking one of the recording beams with an optical shutter (Thorlabs, SHB1T), as shown in Figure 7. The other recording beam was partly diffracted and partly transmitted through the sample with the corresponding powers of P_1 and P_2 measured using a power meter (Ophir, PD300-3W). The diffraction efficiency η can thus be obtained by

$$\eta = \frac{P_1}{P_1 + P_2} \tag{11}$$

5. EXPERIMENTAL RESULTS

5.1. Parameters Fitted by the Photochemical Reaction Model. By measuring η every 30 s during a recording/developing process, Δn_1 can also be obtained by the coupled-wave theory. The data of $\Delta n_1(t)$ can then be fitted by the reaction rate and diffusion equations, thereby determining the unknown material parameters, namely, $D^3_{PQ^*}$, $[H_{react}]_i$, k_i, and γ.

The $\Delta n_1(t)$ of the three PQ/PMMA samples fabricated at T_{evap} = 40 °C with t_{ex} chosen to be 60 s was calculated and plotted in Figure 8. $D^3_{PQ^*}$, γ_{PQ}, $\gamma^3_{PQ^*}$, and $\gamma_{PQ/PMMA}$ of sample 1 were obtained by fitting eqs 6−9 as 3.2×10^{-18} m^2/s, 14.1,

https://doi.org/10.1021/acsomega.1c06887
ACS Omega 2022, 7, 11770−11776

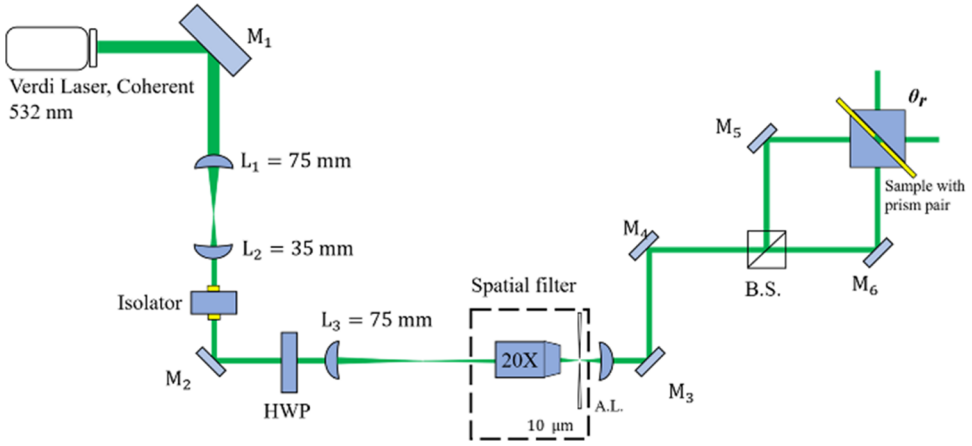

Figure 6. Two-beam interference recording configuration.

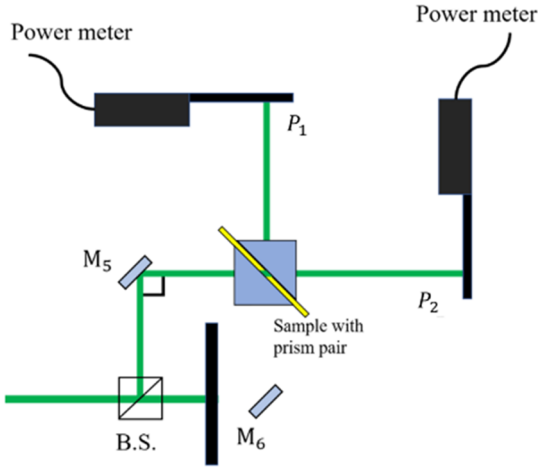

Figure 7. Measurement of the diffraction efficiency of the sample during the recording process.

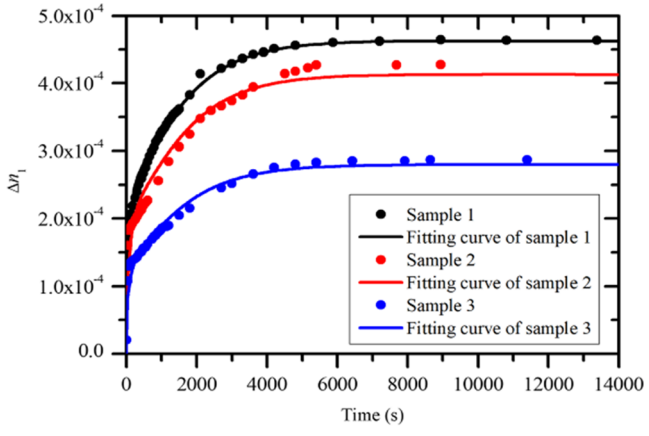

Figure 8. $\Delta n_1(t)$ and the corresponding fitting curves of the three identical PQ/PMMA samples fabricated at T_{evap} = 40 °C with t_{ex} chosen to be 60 s.

16.8, and 37.5 cm^3/mol, respectively. $D^3_{PQ^*}$ and γ are both assumed to be identical under the same fabrication and recording conditions. $[H_{react}]_i$ and k_i listed in Table 3 are the parameters distinguishing different samples. With these values, the fitted $\Delta n_1(t)$ curves agree well with the experimental data of all three samples, as shown in Figure 8. Therefore, under a constant T_{evap}, the assumption of identical values of $D^3_{PQ^*}$ and

Table 3. Parameter Values of the Fitting Curves of Samples 1, 2, and 3

sample	$[H_{react}]_i$ (mol/cm^3)	k_i (cm^3/(mol·s))
sample 1	6.0×10^{-5}	93.9
sample 2	6.7×10^{-5}	56.6
sample 3	6.3×10^{-5}	35.7

γ under the same fabrication and recording conditions is credible.

5.2. Effects of the Evaporation Temperature, T_{evap}. The effects of T_{evap} are analyzed similarly. Totally 57 samples are fabricated at T_{evap} = 60, 40, 25, or 5 °C with the identical recording conditions. $\Delta n_1(t)$ is then obtained and fitted to estimate the material parameters. The recorded samples showed similar weak bleaching at the recording spots, which have no significant difference among different T_{evap} values.

The average $D^3_{PQ^*}$ is plotted against T_{evap} in Figure 9. The trend shows that a lower evaporation temperature leads to a

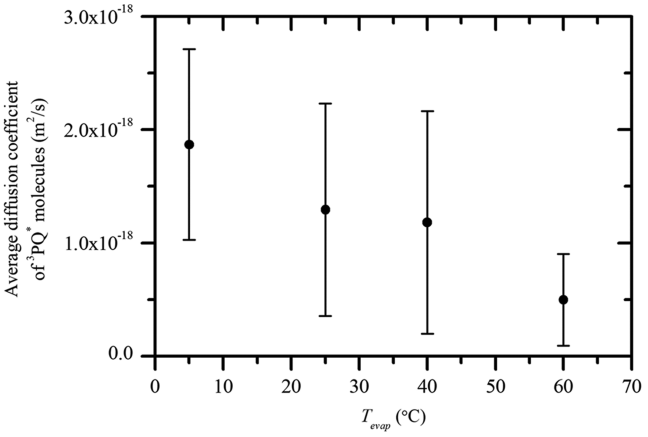

Figure 9. Average $D^3_{PQ^*}$ of a total of 57 PQ/PMMA samples fabricated at different T_{evap} values.

higher value of $D^3_{PQ^*}$. T_{evap} determines the solvent evaporation rate and the kinetic energy of PMMA, which in turn affects the final morphology of the PMMA matrix. A higher value of $D^3_{PQ^*}$ implies that the matrix contains more openings that allow easier diffusion of PQ and $^3PQ^*$ molecules. Therefore, according to Figure 9, lower T_{evap} may tend to result in a

https://doi.org/10.1021/acsomega.1c06887
ACS Omega 2022, 7, 11770−11776

more porous PMMA matrix due to the lack of stretching of PMMA molecules during the process of evaporation.

The calculated k_i versus $[H_{react}]_i$ and $[H_{react}]_i$ versus T_{evap} of all 57 samples are shown in Figure 10a,b, respectively. Most of

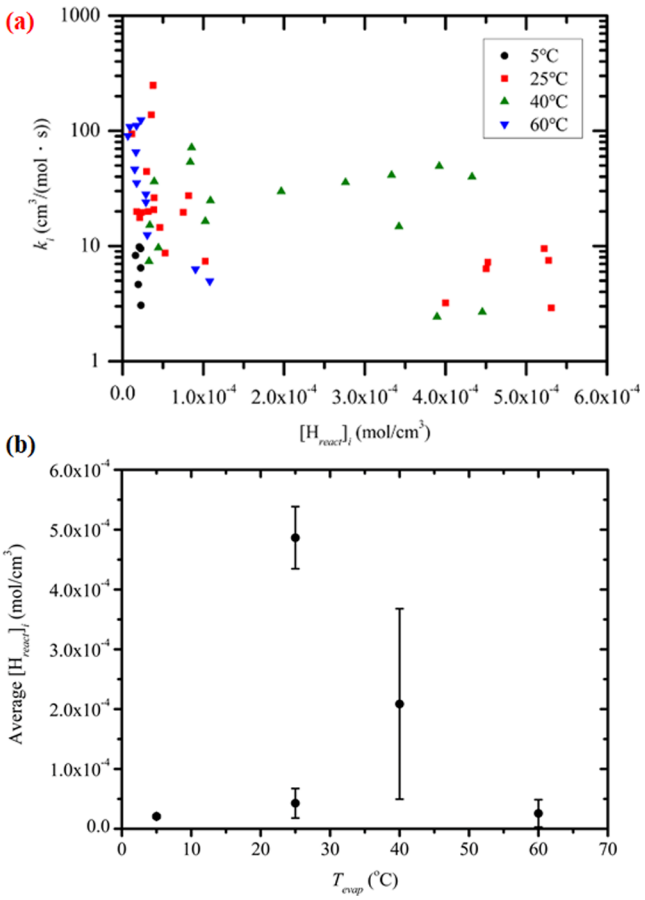

Figure 10. (a) k_i and $[H_{react}]_i$ and (b) average $[H_{react}]_i$ of a total of 57 PQ/PMMA samples fabricated at different T_{evap} values.

the samples have $[H_{react}]_i$ lower than 1×10^{-4} mol/cm^3. However, there are samples with $[H_{react}]_i$ noticeably higher and can even reach 5.3×10^{-4} mol/cm^3. On the other hand, k_i does not show a clear trend and distributes from 3 to 300 cm^3/(mol·s). The data showing higher $[H_{react}]_i$ only appear for T_{evap} = 25 and 40 °C. Though the fabrication and recording conditions are identical, the data of T_{evap} = 25 °C fall into two distinct groups on this plot. About 37% of the samples have high $[H_{react}]_i$ but with low k_i, whereas the other 63% take on lower $[H_{react}]_i$ with relatively high k_i. On the other hand, no conspicuous groups can be found among the data of T_{evap} = 40 °C. Unlike the previous cases, the data of T_{evap} = 5 and 60 °C are confined to relatively small regions with low $[H_{react}]_i$. While $[H_{react}]_i$ almost remains fixed, k_i varies largely.

From the grating fabrication perspective, reaching the highest possible Δn_f and η is the goal. As discussed in Section 3.3, both higher k_i and $[H_{react}]_i$ allow reaching higher Δn_f and η. With T_{evap} = 5 and 60 °C, the samples have low $[H_{react}]_i$ and result in low Δn_f. Though with a minority of the samples fabricated at T_{evap} = 25 °C that have unusually high $[H_{react}]_i$, the fabrication at T_{evap} = 40 °C gives the largest average $[H_{react}]_i$ and Δn_f among the four evaporation temperatures. The average Δn_f of the VBG fabricated at T_{evap} = 40 °C with the previously mentioned recording conditions reached 3.6×10^{-4}. With the same $[PQ]_i$, this value is more than 2 times higher than those of the samples fabricated by the method of two-step thermal polymerization in ref 14, which reached only 1.5×10^{-4}.

At higher T_{evap}, the PMMA matrix may have a chance to settle with fewer pores for PQ to move and less react-able H is exposed. At lower T_{evap}, PQ molecules may tend to cluster. Therefore, PQ may be harder to react. However, the detailed mechanism requires further investigation.

6. CONCLUSIONS

Solvent-cast PQ/PMMA photopolymer films using THF as the solvent are realized with the benefits of fast fabrication, efficient recording, and high refractive index variation. The corresponding photochemical reaction model and the reaction and diffusion equations recorded with a 532 nm laser are established. The fabrication and recording processes can be completed within 4 h. The material parameters $D^3_{PQ^*}$, $[H_{react}]_i$, k_i, and γ are numerically obtained and analyzed based on 57 samples. With a 40 °C evaporation temperature, 96 J/cm^2 recording fluence, and 60 s exposure time, the average Δn_f of such PQ/PMMA films can reach 3.6×10^{-4}.

AUTHOR INFORMATION

Corresponding Author

Te-yuan Chung − *Department of Optics and Photonics, National Central University, Taoyuan City, Taiwan 32001;* orcid.org/0000-0002-5915-5483; Email: tychung@dop.ncu.edu.tw

Authors

Yu-Hsiang Hsieh − *Department of Optics and Photonics, National Central University, Taoyuan City, Taiwan 32001*

Yung-Cheng Cheng − *Department of Optics and Photonics, National Central University, Taoyuan City, Taiwan 32001*

Complete contact information is available at: https://pubs.acs.org/10.1021/acsomega.1c06887

Author Contributions

Y.-C.C. carried out the simulation, experiment, and fundamental analysis; Y.-H.H. refined the analysis and wrote the manuscript; and T.-Y.C. supervised the research. All authors provided critical feedback and discussed the results that contributed to the final manuscript.

Funding

The Ministry of Science and Technology, Taiwan (MOST 108-2221-E-008-085-MY3).

Notes

The authors declare no competing financial interest.

ACKNOWLEDGMENTS

The authors would like to thank Prof. Lin, Shiuan-Huei for his generous help and valuable discussion.

REFERENCES

(1) Steckman, G. J.; Solomatine, I.; Zhou, G.; Psaltis, D. Characterization of phenanthrenequinone-doped poly(methyl methacrylate) for holographic memory. *Opt. Lett.* **1998**, *23*, 1310−1312.

(2) Lin, S. H.; Hsu, K. Y.; Chen, W. Z.; Whang, W. T. Phenanthrenequinone-doped poly(methyl methacrylate) photopolymer bulk for volume holographic data storage. *Opt. Lett.* **2000**, *25*, 451−453.

(3) Mumbru, J.; Solomatine, I.; Psaltis, D.; Lin, S. H.; Hsu, K. Y.; Chen, W. Z.; Whang, W. T. Comparison of the recording dynamics of phenanthrenequinone-doped poly(methyl methacrylate) materials. *Opt. Commun.* **2001**, *194*, 103−108.
(4) Hsu, K. Y.; Lin, S. H.; Hsiao, Y. N.; Whang, W. T. Experimental characterization of phenanthrenequinone-doped poly(methyl methacrylate) photopolymer for volume holographic storage. *Opt. Eng.* **2003**, *42*, 1390−1396.
(5) Veniaminov, A. V.; Bandyuk, O. V.; Andreeva, O. V. Materials with diffusion amplification for optical-information recording and their study by a holographic method. *J. Opt. Technol.* **2008**, *75*, 306−310.
(6) Liu, P.; Chang, F. W.; Zhao, Y.; Li, Z. R.; Sun, X. D. Ultrafast volume holographic storage on PQ/PMMA photopolymers with nanosecond pulsed exposures. *Opt. Express* **2018**, *26*, 1072−1082.
(7) Manukhin, B. G.; Chivilikhin, S. A.; Andreeva, N. V.; Kuzmina, T. B.; Materikina, D. A.; Andreeva, O. V. Reversible and irreversible alterations of the optical thickness of PQ/PMMA volume recording media samples. Part 2: mathematical modeling. *Appl. Opt.* **2018**, *57*, 9406−9413.
(8) Luo, Y.; Gelsinger, P. J.; Barton, J. K.; Barbastathis, G.; Kostuk, R. K. Optimization of multiplexed holographic gratings in PQ-PMMA for spectral spatial imaging filters. *Opt. Lett.* **2008**, *33*, 566−568.
(9) Hsieh, Y. H.; Chung, T. Y.; Du, L. C.; Lin, S. H. A High Power, Narrow Linewidth and Wavelength Tunable Semiconductor Laser using a Photopolymer Bragg Grating as One of the Cavity Mirrors. In *Frontiers in Optics 2014/Laser Science XXVII*; Tucson: AZ, USA, 2014.
(10) Liu, S.; Gleeson, M. R.; Guo, J.; Sheridan, J. T.; Tolstik, E.; Matusevich, V.; Kowarschik, R. Modeling the photochemical kinetics induced by holographic exposures in PQ/PMMA photopolymer material. *J. Opt. Soc. Am. B* **2011**, *28*, 2833−2843.
(11) Shih, B. J.; Chen, C. W.; Hsieh, Y. H.; Chung, T. Y.; Lin, S. H. Modeling the Diffraction Efficiency of Reflective-Type PQ-PMMA VBG Using Simplified Rate Equations. *IEEE Photonics J.* **2018**, *10*, 1−7.
(12) Diao, Y.; Shaw, L.; Bao, Z.; Mannsfeld, S. C. B. Morphology control strategies for solution-processed organic semiconductor thin films. *Energy Environ. Sci.* **2014**, *7*, 2145−2159.
(13) Qi, Y.; Tolstik, E.; Li, H.; Guo, J.; Gleeson, M. R.; Matusevich, V.; Kowarschik, R.; Sheridan, J. T. Study of PQ/PMMA photopolymer. Part 2: experimental results. *J. Opt. Soc. Am. B* **2013**, *30*, 3308−3315.
(14) Chung, T. Y.; Hsu, W. T.; Hsieh, Y. H.; Shih, B. J. Recording 2nd order PQ:PMMA reflective VBG for diode laser output spectrum narrowing. *Opt. Express* **2019**, *27*, 8258−8266.
(15) Gleeson, M. R.; Sheridan, J. T. Nonlocal photopolymerization kinetics including multiple termination mechanisms and dark reactions. Part I. Modeling. *J. Opt. Soc. Am. B* **2009**, *26*, 1736−1745.
(16) Kogelnik, H. Coupled Wave Theory for Thick Hologram Gratings. *Bell Syst. Tech. J.* **1969**, *48*, 2909−2947.
(17) Lin, P. J.; Hsieh, Y. H.; Chung, T. Y. Modeling the reaction of PQ:DMNA/PMMA photopolymer recorded at 640 nm. *Opt. Mater. Express* **2021**, *11*, 2608−2617.
(18) Drioli, E.; Giorno, L., *Membrane Operations: Innovative Separations and Transformations*; John Wiley & Sons, 2009.
(19) Lim, J. A.; Lee, H. S.; Lee, W. H.; Cho, K. Control of the morphology and structural development of solution-processed functionalized acenes for high-performance organic transistors. *Adv. Funct. Mater.* **2009**, *19*, 1515−1525.
(20) Liu, S.; Wang, W. M.; Briseno, A. L.; Mannsfeld, S. C. B.; Bao, Z. Controlled deposition of crystalline organic semiconductors for field-effect-transistor applications. *Adv. Mater.* **2009**, *21*, 1217−1232.
(21) Virkar, A. A.; Mannsfeld, S.; Bao, Z.; Stingelin, N. Organic semiconductor growth and morphology considerations for organic thin-film transistors. *Adv. Mater.* **2010**, *22*, 3857−3875.

https://doi.org/10.1021/acsomega.1c06887
ACS Omega 2022, 7, 11770−11776